Characterization of Batch Mixers Using Numerical Flow Simulations

T. Jongen
Unilever Research, 3133 AT Vlaardingen, The Netherlands

The objective of this work is to characterize various deformations to which viscous pastes are subjected during their batch mixing and to investigate the influence of mixer configurations and operating conditions. For this, several mixer geometries were modeled in a way representative of the mixing mechanisms taking place. The twin-blade arrangement, which is typical in batch mixing, was used in this study, as well as planetary mixers. The equations governing the deformation of the fluid were solved in the various mixer geometries, using numerical solution techniques (finite-element discretization on a fixed mesh, with a fictitious domain method accounting for the internally moving blades). Based on the time-dependence velocity fields obtained, the type of deformation taking place in various mixers was characterized using relevant kinematic flow classification parameters. These parameters were then related to the mechanical action of the mixer.

Introduction

Mixing in many industrial processes is used for homogenization, where multiple components have to be mixed together into a homogeneous mixture. This subject has been extensively studied for many decades, and quantities such as scales and intensity of separation of the mixture, mixing efficiency, mixing times, and power consumption have been investigated theoretically and experimentally (Irving and Saxton, 1967; Godfrey, 1986; Ottino, 1989; Tanguy et al., 1992, 1996). However, there are processes where the aim of mixing is not blending, but rather development of a material in the mixer. This is particularly relevant for the processing of many pastes (such as food stuff or complex (bio)polymers in the food, pharmaceutical, or chemical industries) where it is not so much the mixing action (homogenization) taking place in the mixer that matters, but rather the way in which the deformation is provided to the material. Deformations have a large influence on the structure and the development of the material, and it is very important to be able to relate these properties to the mechanical action of the mixer. The following observations are for instance typical of the mixing of many viscous materials containing (bio)polymers:

(a) The action of the mixer is to transfer a given amount of energy into the material in order to transform and develop it to an optimum.

(b) The way in which this energy is transferred is crucial. For instance, with the same amount of energy transferred, a paste mixed using only shearing will be totally different from a paste developed using only elongational deformations.

Assuming that, for a given material, the optimal type of deformation needed is known (through experiments, for instance), the complementary design step is to develop mixers which provide this type of deformation preferentially. However, for this, it is necessary to identify the relation between the mixer and the type of deformation it provides. This is the objective of the present study, where the deformation provided by different mixers will be characterized. Global and detailed modeling approaches are discussed. For the latter, the governing equations, as well as the flow characterization parameter, are defined. The different mixers to be simulated are described, and the results are presented with commentary. Finally, some conclusions are drawn.

Modeling Approaches

As stated in the introduction, two types of questions are important when studying the mixing of viscous pastes: how much energy is transferred into the material during mixing, and how is this energy transferred.

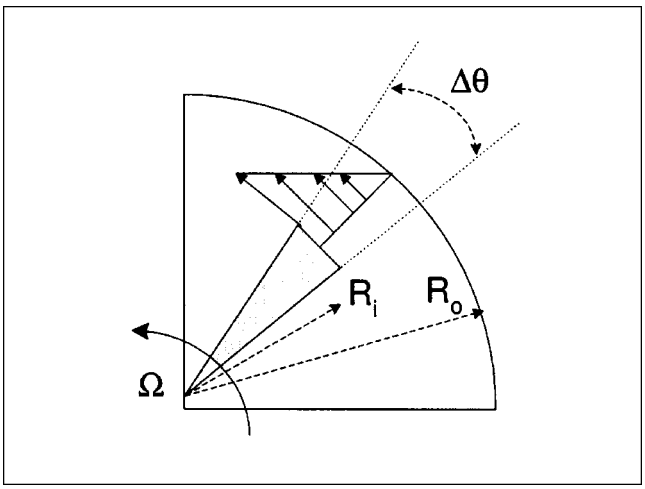

Figure 1. Global parametrization: typical blade-mixer system and relevant parameters used to compute the energy input into the material.

Global parameterization

The first type of question can be answered by studying the energy transfer as a function of several macroscopic kinematic and process quantities such as mixing time and power consumption. It is possible to develop global parametric relations involving the energy transfer using simple mechanical considerations (Godfrey, 1986). For instance, for a given mixer configuration, the mixing time t required to transfer the amount of energy Q into the material can be formally expressed as

$$t = F(Q, W, \epsilon, \ldots) \tag{1}$$

where W is the rate of energy transfer from the mixer into the paste, and ϵ is a mixing efficiency, characteristic of the type of deformation with which the energy is transferred from the mixer to the material. The actual form of the relationship F depends on the mixer configuration and on the operating conditions. As a simple illustration, the energy transfer associated with a pure shearing flow in the clearance between a blade and the mixer wall can be parameterized as follows (see Figure 1)

$$Q = 2^n \pi^{n-1} \frac{\Delta\theta}{(R_o - R_i)^n} \left(\frac{R_o}{R_i}\right)^2 \frac{\mu_0}{\rho} \Omega^{n+1} t \tag{2}$$

for a power-law fluid, with power-law index n, and consistency index μ_0. When rewritten in form 1, relation 2 gives the parametric relationship between the mixing time t, energy input Q, mixer geometry R_i, R_o, $\Delta\theta$, operating conditions ϵ, and material rheology μ_0, ρ.

Detailed kinematic analysis

The second question—the *how* rather than the *how much*—requires the detailed study of the flow pattern of the material inside the mixer during processing, and the further extraction of the relevant deformation characteristics. For this, computational fluid dynamics (CFD) simulations are used to obtain the deformation field via computer simulations. The equations governing the flow of the fluid in the mixer configurations are discretized, and the corresponding systems of equations are solved using computer techniques. As a result, the space and time distribution of the velocity field is obtained, and the type of deformation can be deduced from it.

Governing Equations. The flow of an incompressible fluid in a domain Ω with boundaries Γ is governed by the classical Navier-Stokes equations (Bird et al., 1977) expressing momentum and mass conservation

$$\begin{cases} \dfrac{\partial}{\partial t} u_i + u_j \dfrac{\partial}{\partial x_j} u_i = -\dfrac{1}{\rho} \dfrac{\partial}{\partial x_j} (p\delta_{ij} + \tau_{ij}) \\ \qquad\qquad\qquad\qquad\qquad\qquad \text{in } \Omega \\ \dfrac{\partial}{\partial x_i} u_i = 0 \end{cases} \tag{3}$$

where the summation convention over repeated indices has been used. In Eq. 3, u_i are the velocity components, ρ is the fluid density, and p is the pressure. The stress tensor τ_{ij} is a function of the velocity field, which is expressed by a constitutive equation. We restrict ourselves here to Newtonian flows having a simple constitutive relation of the form

$$\tau_{ij} = -2\mu S_{ij} \tag{4}$$

where μ is the constant fluid dynamic viscosity. The study to be presented in this article could however be equally well applied to pastes having a more complex rheology. The strain rate tensor S and the rotation rate tensor W are defined by

$$S_{ij} = \frac{1}{2}\left(\frac{\partial}{\partial x_j} u_i + \frac{\partial}{\partial x_i} u_j\right) \text{ and } W_{ij} = \frac{1}{2}\left(\frac{\partial}{\partial x_j} u_i - \frac{\partial}{\partial x_i} u_j\right) \tag{5}$$

The governing Eqs. 3 must be solved together with the appropriate boundary conditions on Γ over a given time interval $t \in T$. For this, the equations are discretized using a Galerkin finite-element approximation technique, and the resulting sets of algebraic equations are solved on a computer. In this study, the FIDAP 8.0 CFD simulation software has been employed (FIDAP, 1993). For the two-dimensional (2-D) flow domains used here, bilinear four-nodes quadrilateral elements have been used.

A common feature of virtually all the batch mixers is the presence of moving parts inside the mixing vessel. These elements deform and mix the material by constraining the motion around it. In some instances, it is possible to attach a new reference frame to the moving parts, in such a way that when expressed in the new co-ordinate system, the velocity field is stationary. In this case, the problem is greatly simplified since only a steady-state solution must be computed. Anticipating from the next section, one salient feature of the

mixer configurations to be studied here is that it is not possible to find such a reference frame in which the velocity field would be stationary. Consequently, the full-time history of the flow must be tracked, and internally moving parts must be explicitly accounted for. Using a variant of the recently introduced fictitious domain method (Glowinski et al., 1994; Bertrand et al., 1997), the moving internal parts of the geometry are not meshed as such. Instead, they are taken into account by means of a set of pointwise kinematic constraint that is coupled with the questions of motion (FIDAP, 1993). Velocity constraint is imposed on the degrees of freedom, so that only kinematics of the moving parts must be known *a priori*. More specifically, if at time t, the mesh node x^k is covered by the moving body, then the velocity degree of freedom u_i^k corresponding to this node receives the prescribed value of the velocity of the moving body over the integration time interval. As the position in time of the moving body is known *a priori*, the algorithm for deciding whether a mesh node is covered or not by the body at a given time can be designed beforehand, and used as an input for the computations. In the FIDAP implementation, the exact location of the boundary of the moving body is known up to one mesh cell thickness, as partial coverage of the cell by the body is not taken into account (a mesh node is covered or not, at a given time). This results in a loss of accuracy close to the boundary of the moving body, which acts effectively as a (time-dependent) rough surface. This effect can, however, be minimized by using small enough mesh elements. Tests have been performed with various mesh densities, which showed that smoothness of the fields away from the body's boundaries was achieved rapidly.

Flow Type Characterization. The knowledge of the space and time evolution of the velocity field enables us to derive parameters that characterize the type of deformation taking place in the mixer. Intuitively, one can distinguish between three extreme cases of flow types that may be encountered. At one extreme lie the purely extensional flows, which are strong flows where the material lines are largely deformed. On another extreme lie the shear flows (viscometric flows), and the third class is represented by rigid-body motions, or solid-body rotations, which do not generate any deformation in a fluid. Following Astarita (1979), it would be useful to be able to calculate, for any flow pattern, a criterion whose value identifies the flow considered in terms of the types mentioned above. It can be argued that such a flow-type criterion should fulfill several properties: locality (that is, one should be able to indicate its value at a point, rather than in a flow volume), objectivity (invariance under a change of reference frame), and generality of application (its value should be always available, and should make sense for any conceivable local kinematics). In addition, a scalar-valued criterion is preferred, since only the type of flow is needed in the present context, without directional information. Finally, this criterion should in the first instance be dependent only on the kinematics of the motion, and not on the nature of the fluid. A number of such flow classification criteria have been proposed. This is a subject of much controversy, and extensive discussions about the existence and suitability of such a flow parameter can be found in Astarita (1979), Huigol (1980), Olbricht et al. (1982), Ottino (1989), and Schunk and Scriven (1990).

The flow parameter definition which has been retained here is based on the invariants of the velocity gradient tensor (Astarita, 1979). The shear rate parameter s^2 is defined as the second invariant of the strain rate tensor (see Eq. 5),

$$s^2 = \text{trace}\,(S^2) = S_{mn}S_{nm} \tag{6}$$

and the rotation rate parameter ω^2 is defined in a similar way as

$$\omega^2 = -\,\text{trace}\,(W^2) = -\,W_{mn}W_{nm} \tag{7}$$

These parameters can serve as a measure of the deformation intensity. The ratio of these two quantities can be used as a flow parameter

$$\mathfrak{R}^2 = \frac{\omega^2}{s^2} = -\,\frac{W_{mn}W_{nm}}{S_{mn}S_{nm}} \tag{8}$$

which can be further normalized by (Ottino, 1989)

$$D = \frac{1-\mathfrak{R}^2}{1+\mathfrak{R}^2} \tag{9}$$

Thus, $D \in [-1, 1]$ and takes the following values in particular: $D = -1$ for pure rotational flow, $D = 0$ for a pure shear flow, and $D = +1$ in a pure extensional flow. Note that criterion 9 is strictly valid for planar flows only, and generalizations to fully 3-D flows are ambiguous and not trivial (Olbricht et al., 1982). Also, criterion D does not fulfill the objectivity requirement. A number of alternative criteria have been proposed (Astarita, 1979). We argue here that for the sole purpose of flow classification, the objectivity requirement is not essential because it is not used to derive constitutive relations, and we prefer to keep the simplicity of criteria 9. The various mixers are analyzed in an inertial reference frame and, under this restriction, comparisons of the values of the D parameter are possible and meaningful, which is not the case if this parameter is used to analyze some of the mixers in a noninertial reference frame. Note, however, that if such a flow parameter should be used in the expression of a material constitutive relation, then the objectivity requirement could not be discarded (Schunk and Scriven, 1990).

Mixer Configurations

Three mixer configurations have been selected for the present study. A sketch of the mixers is given on Figure 2. In the plastograph mixer (Figure 2a) two blades are mounted on parallel horizontal shafts, and are contra-rotating inside a closed cavity (Kawaguchi et al., 1997). The geometrical parameters are set as follows: $L/W = 2.1$, $R_o/W = 0.49$, $R_B/W = 0.47$, and $H/W = 0.61$. During operation, the two blades are rotating at different rotational speeds, $\omega_1 = 3/2\,\omega_2$, with

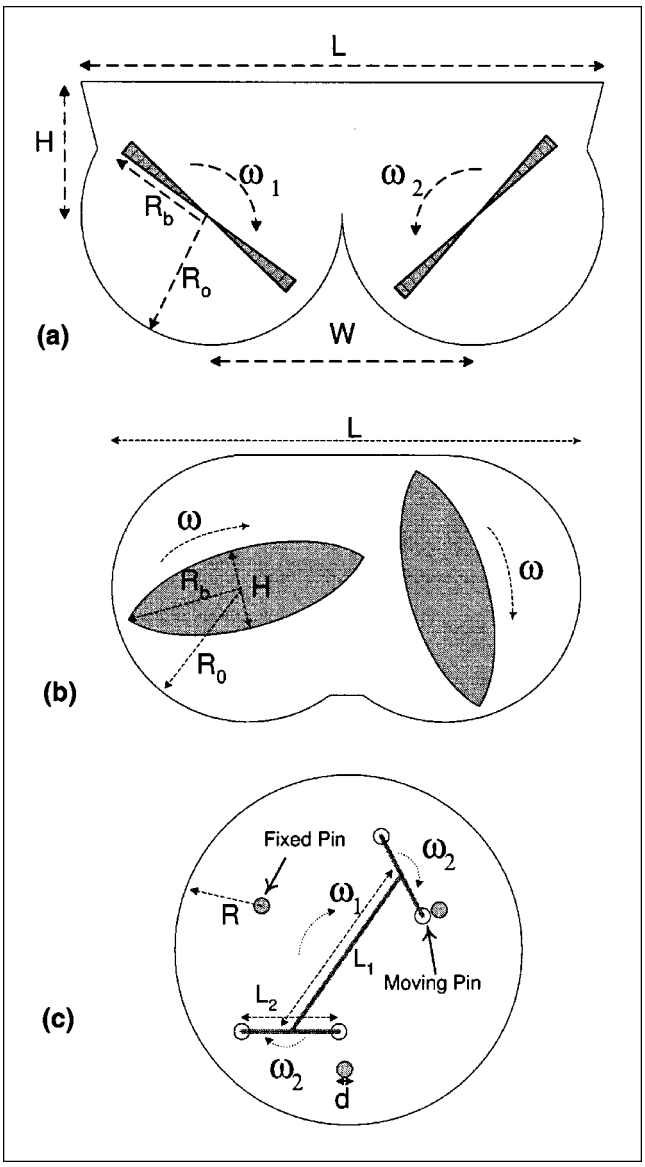

Figure 2. Geometry of the mixers considered in this study.

(a) Plastograph; (b) do-corder; (c) planetary mixer.

$\omega_2 = 1.033$ RPS. For the do-corder mixer (Figure 2b), a twin-blade arrangement is used, where the blade rotation domains are interpenetrating and co-rotate in a bowl shaped to keep blade to wall clearance low. The mixer geometrical parameters are set as follows: $H/L = 0.1$, $R_o/L = 0.32$, and $R_b/L = 0.3$. The two blades are rotating at the same speed, $\omega = 1$ RPS. Finally, the planetary mixer (Figure 2c) has a complex motion induced by a main arm rotating about an axis passing through the center of the mixing vessel. This arm supports two gears equipped with a pair of vertical pins. The combined motion of the central arm and the pins induces a planetary-type motion, where the pins span a large portion of the mixing bowl (Buchholz, 1990). Planetary mixer dimensions are set as follows: $L_2/L_1 = 0.6$ and $R/L_1 = 1.1$. The rotation speeds are $\omega_1 = 1.37$ RPS and $\omega_2 = 2.39$ RPS.

For all the mixers presented above, the flow will essentially be 2-D, and will take place inside sections perpendicular to the rotation axes of the moving parts (neglecting end effects). In this case, a 2-D, time-dependent simulation would be sufficient, since there is no axial flow. As already mentioned, the attention is restricted to highly viscous pastes having a Newtonian behavior. For all the simulations presented below, the dynamic viscosity μ has been set to a very high value (such that representative Reynolds numbers based on mixer dimensions and rotation speeds are $Re \equiv 10^{-5}$ [Pa·s]).

Simulation Results

The mixer geometries described above have been discretized on finite-element meshes covering the whole mixing volume, and do not account for the presence of the blades or mixing elements. As explained above, the presence of these solid bodies is accounted for by imposing time-dependent constraint to the mesh elements covered by the bodies at each time, which has the tremendous advantage of allowing for extremely simple and accurate grids. For these time-dependent flows, mesh densities result from a compromise between computational time requirements and accuracy, and varies between 9,874 elements for the planetary mixer to 49,473 elements for the plastograph mixer. For all the mixers, the computations have been carried out over several revolutions until periodicity of the flow field was established. Time-averaged quantities presented hereafter are based on results where periodicity of the flow field was achieved. Note that owing to the extreme value of the viscosity, periodicity was in all the cases already virtually achieved after the first cycle of blade rotation of the mixers.

As explained in the previous section, the objective of this study is to investigate the dependence of the paste deformation characteristics upon mixer types and operating conditions (rotation speed, tip clearance, ... of the blades). The scalar parameter D, defined in Eq. 9, enables us to distinguish between flow types (rotation, shear, and elongation) independently of the deformation intensity and orientation. As an illustration, the instantaneous distribution of the parameter D is given in Figure 3 for the plastograph, and its evolution in time for all mixers considered is sketched on Figures 4–6. Clearly, distinct features can be identified for the different mixers. As expected, regions near the moving parts and the walls of the mixers have a pronounced shear characteristic (such as in the blade clearances for the plastograph and the do-corder; in the region between the moving and the stationary pins for the planetary mixer). Large rotational zones are also clearly present for some mixers. In the plastograph, the region around the blades is predominantly rotational. When tracked in time, this region seems to be literally attached to the mixer blades, and rotates with them (Figure 4). One can already conclude that this represents a "dead" region, where the material is not deformed (solid-body rotation), but merely rotates with little exchange with the rest of the flow domain. The evolution of material elements acting as tracers injected in the mixer are shown in Figure 7. As they are entrained by the blades, they are displaced over distance comparable to the total blade displacement, with little exchange from one side of the mixer to the other one. For

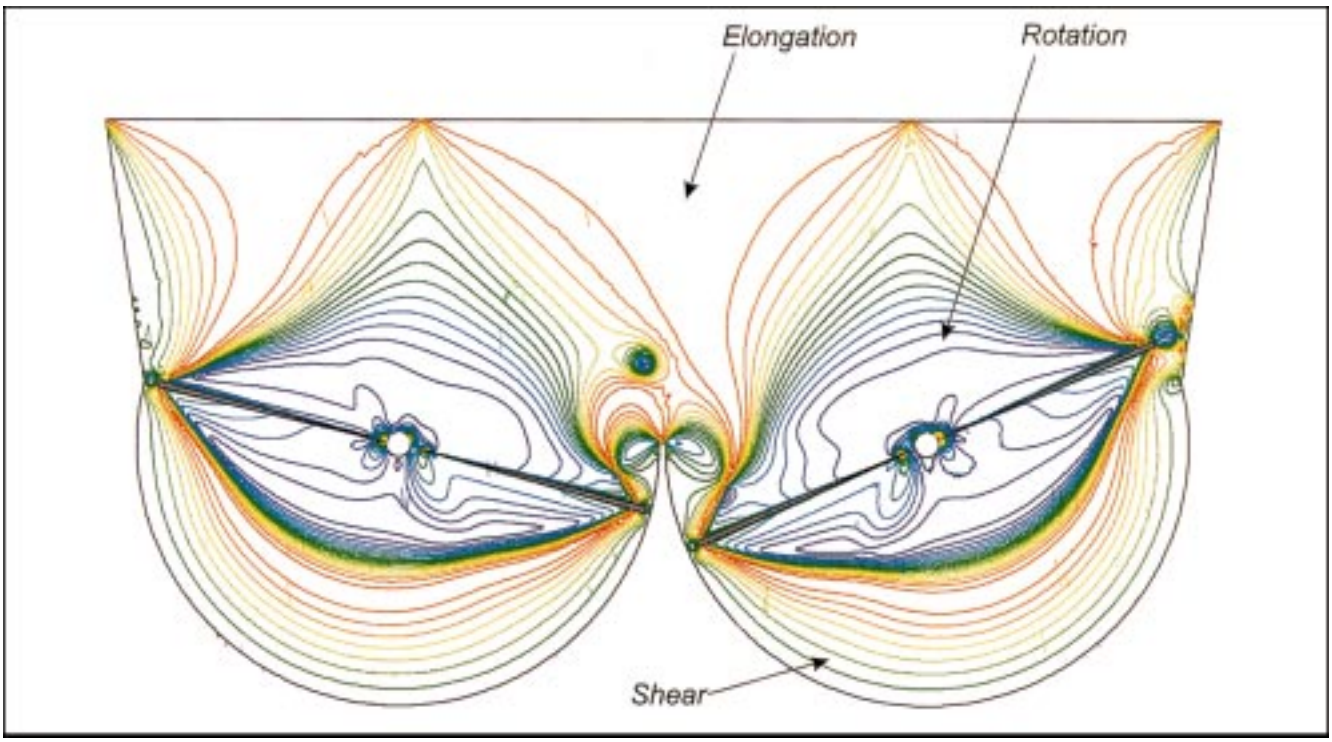

Figure 3. Example of instantaneous spatial distribution of the flow-type parameter *D* in the plastograph.

Contour values are uniformly distributed within a range between blue (rotation, $D = -1$), green (shear, $D = 0$) and red (elongation, $D = 1$).

the do-corder, on the other hand, rotational zones are almost absent, and most of the flow is subjected to elongation and shearing. In fact, the only significant rotation occurs in a small layer between the tip of the blades and the cavity wall, where a kind of ''vortex'' seems to be attached to the blade tips. This rotational zone could be thought of as a small ''roller'' caused by the competition between two effects: on the one hand, the material is entrained by the moving blades, but on the other hand, there cannot be an overall entrainment in the blade clearance because of the presence of the other blade. By incompressibility, some of the material has to flow in the other direction relative to the blade, hence, the rotational zone. This effect can be clearly seen when following in time the position of material elements in the paste (Figure 8). Although tracers injected in the neighborhood of the left blade have an overall displacement in the same direction as the rotation of the blade (clockwise on the figure), tracers injected in the right region have an overall displacement in the *opposite* direction from the direction of rotation of the right blade (clockwise on the figure). This effect results from the fact that there is an overall entrainment of fluid towards the upper region of the mixing cavity, and through the interblade region, where the material is stretched and sheared towards the bottom of the mixer. Due to the slight asymmetry of the cavity (the top middle part of the mixer is different from the bottom part), the system has ''chosen'' for this flow direction, whereas in a perfectly symmetric configuration, the system would have been unable to ''choose'' between two equally valid flow solutions: flow in the same direction as the rotation of the left (resp. right) blade, with counterflow around the right (resp. left) blade and forcing through the interblade zone from top (resp. bottom) to bottom (resp. top). In the present configuration, all the tracers initially placed along the vertical line of symmetry of the mixer will move from top to bottom through the interblade region, and will then loop around the blades to come back in the elongation zone at the top. Only the tracer initially placed at the bottom of the mixer will remain there indefinitely, even if the ''roller'' and the shear layer periodically pass over it (Figure 5). The region of bad mixing and limited paste development in the bottom middle part of the mixer is frequently observed experimentally, where the initial components of the paste are found intact at the end of the process. It is also interesting to note that the blades of the do-corder mixer have a very similar shape as the shape of the rotational zone in the plastograph. One could therefore conclude that the rotational ''dead'' zone in the plastograph has been replaced by the solid material of the blades in the do-corder.

As shown in Figure 6, the material in the planetary mixer is mainly subjected to shearing and elongation between the moving pins, the bowl, and the static pins. The particle tracer trajectories cover virtually all of the mixing region, and are mainly circumferential, with sharp changes in direction for tracers present in the central part of the mixing bowl as a moving pin passes close to the tracer location, and entrains it (Figure 9).

As already apparent from the space and time distributions of the deformation parameter *D*, clear differences exist between the action of the mixers. In order to have a more quantitative way to assess these differences over the whole

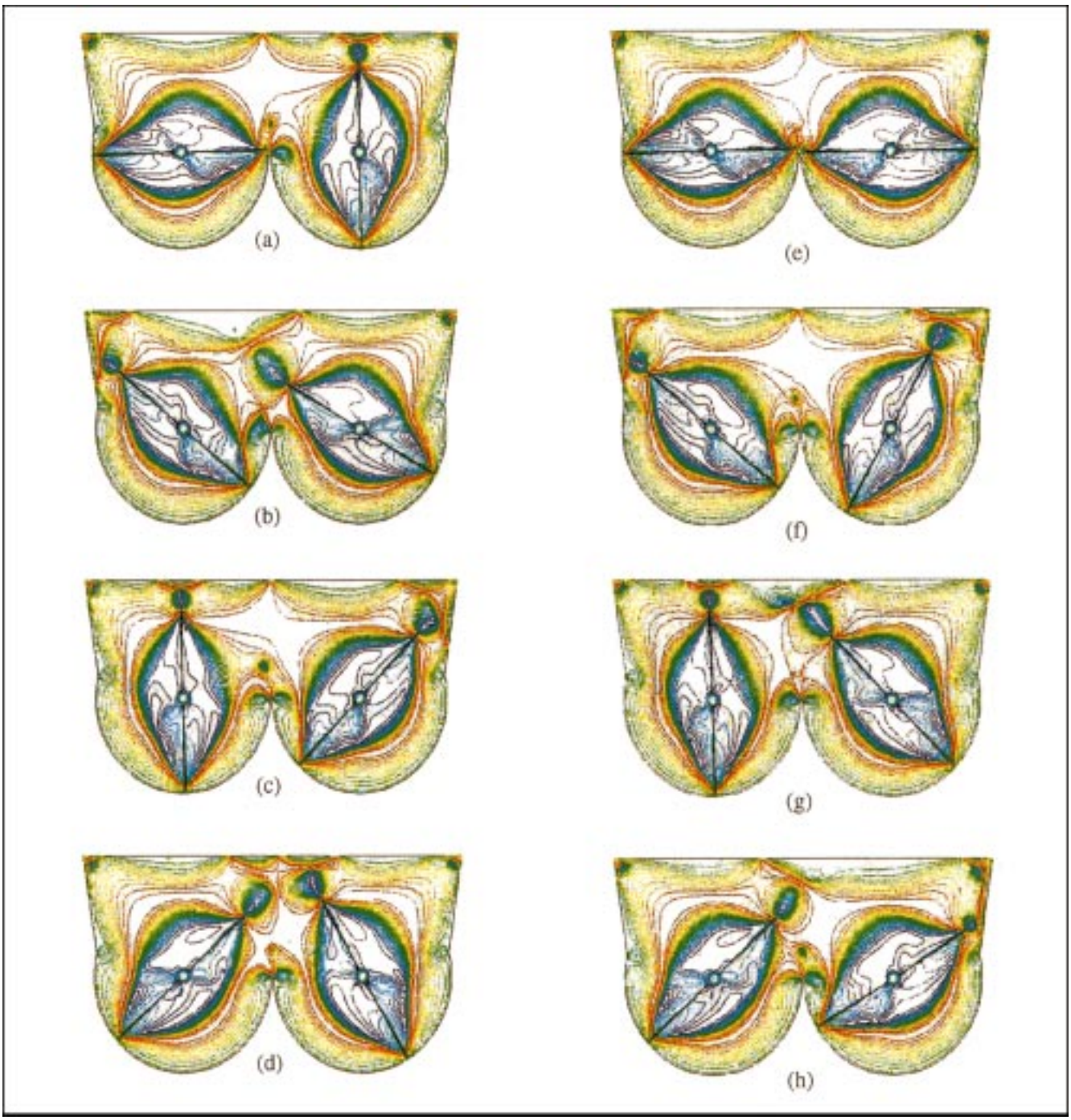

Figure 4. Sequence of instantaneous distributions of the flow-type parameter *D* in the plastograph over one rotation of the slow blade.

The time interval between the figures is constant, and corresponds to $1/8T$, where T is the period of rotation of the slow blade. Contour values are uniformly distributed within a range between blue (rotation, $D = -1$), green (shear, $D = 0$) and red (elongation, $D = 1$).

operation time of the mixers, several averaged quantities can be defined. First, the space-averaged distribution of the parameter D, defined as

$$\langle D \rangle = \frac{1}{S} \int_{\Omega} D(., t)\, dS \qquad (10)$$

can be investigated, where S is the mixing cavity cross-section area and $\langle D \rangle$ is a function of time only. Its evolution will be shown in Figure 12 for the different mixers considered in this study. The periodicity of the flow is clearly visible. The frequency distribution of the flow parameter can also be used for mixer characterization. For this, we define the frequency function

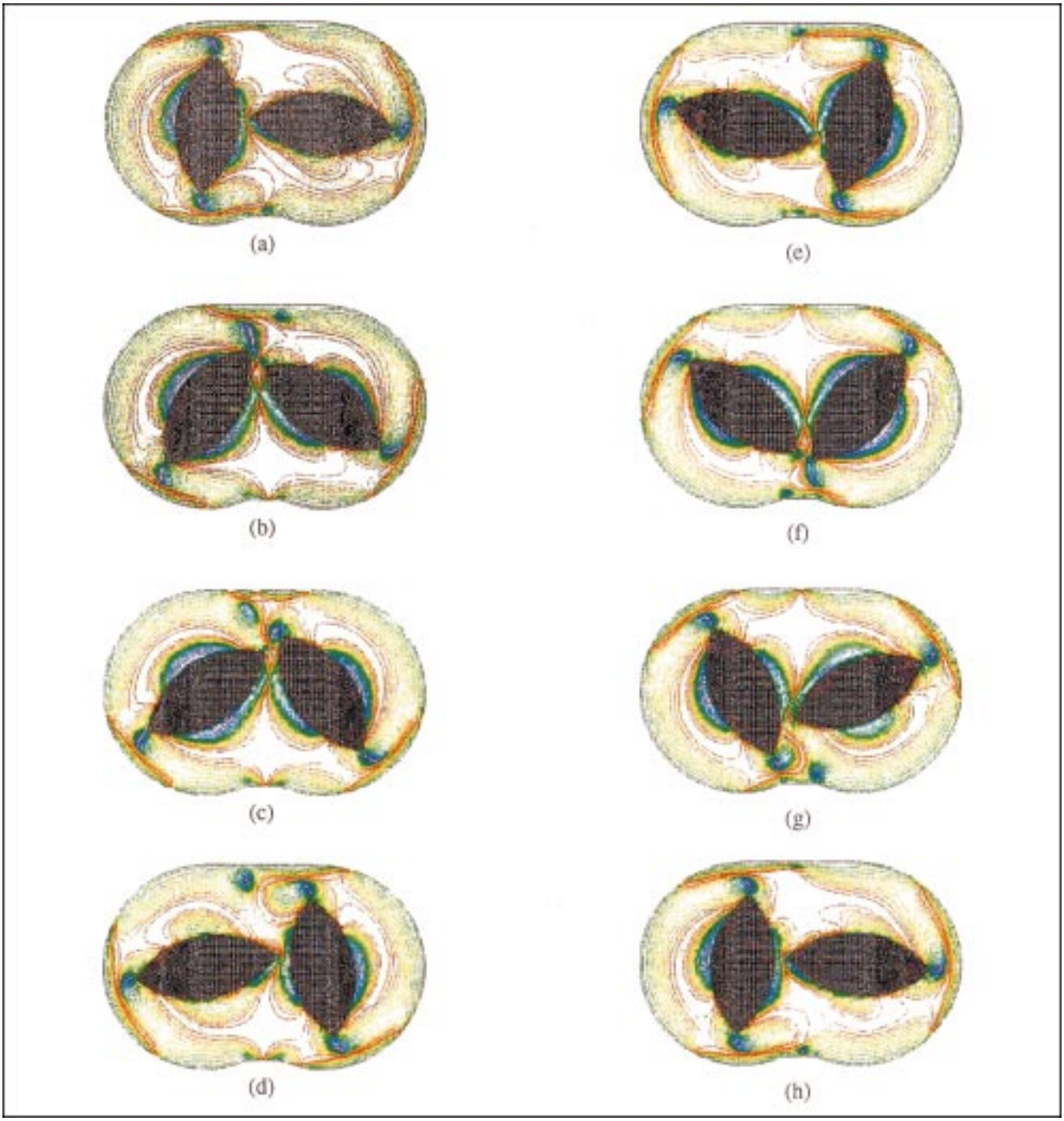

Figure 5. Sequence of instantaneous distributions of the flow-type parameter *D* in the do-corder over one-half rotation of the blades.

The time interval between the figures is constant, and corresponds to 1/14T, where T is the period of rotation of the blades. Contour values are uniformly distributed within a range between blue (rotation, $D = -1$), green (shear, $D = 0$), and red (elongation, $D = 1$).

$$f(D,t) = \frac{dS_{D,t}}{S} \tag{11}$$

$$\tilde{f}(D) = \frac{1}{T}\int_0^T f(D,t)\,dt \tag{12}$$

where $dS_{D,t}$ is the total area of fluid material that is subjected to a deformation between D and $D + dD$ at time t. Define now the time-averaged quantity

where T is the period of the flow (that is, of the mixer). The function $\tilde{f}(D)$ represents the proportion of the fluid volume which—on the average—is subjected to a deformation D.

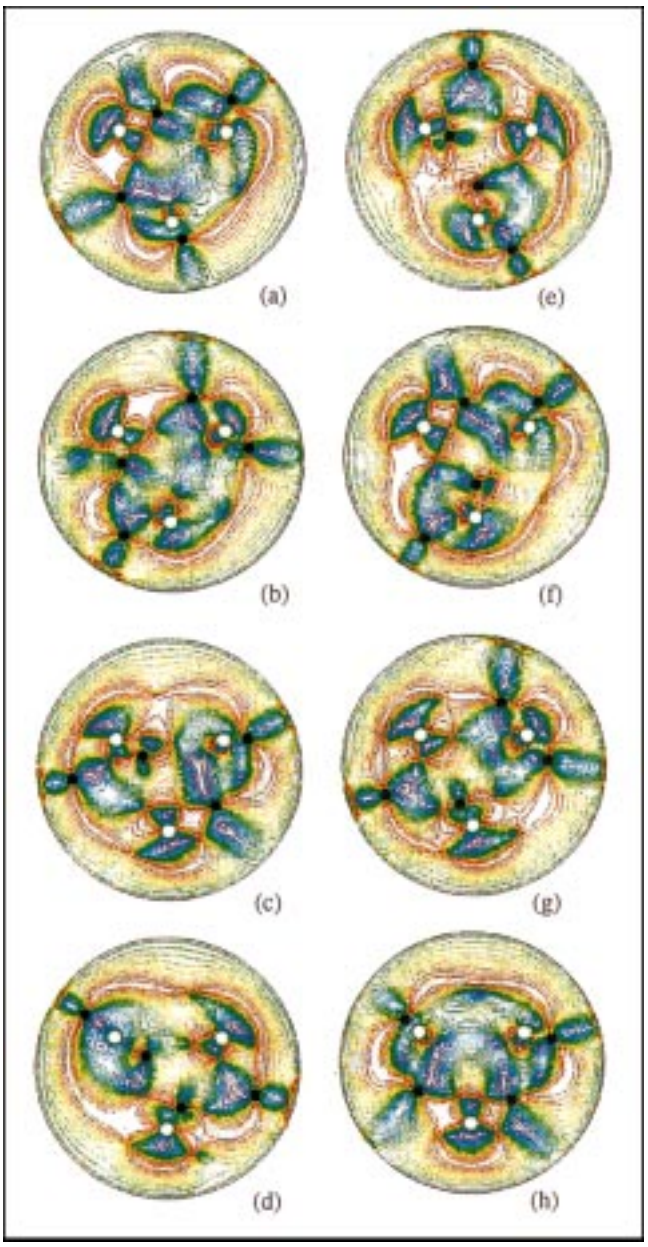

Figure 6. Sequence of instantaneous distributions of the flow-type parameter *D* in the planetary mixer over one rotation of the main supporting arm.

The time interval between the figures is constant, and corresponds to $1/8T$, where T is the period of rotation of the main arm. Contour values are uniformly distributed within a range between blue (rotation, $D = -1$), green (shear, $D = 0$) and red (elongation, $D = 1$).

Graphs of the frequency function $\bar{f}$ are shown in Figure 10. Note that in the figure, the function $\bar{f}$ has been scaled so that the area comprised under the curve equals unity (thus, $\bar{f}/dD$ is actually shown). As already discussed, based on qualitative considerations, the do-corder shows the most elongational flow, with very little rotation. The planetary mixer has the most pronounced shear component, with little rotation as well. The plastograph has a significant rotational part with

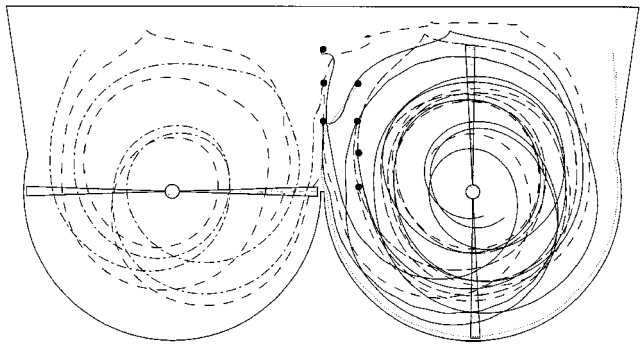

Figure 7. Particle path in the plastograph over three periods of rotation of the mixer.

Initial tracer positions are identified by the filled circles in the mixer.

the shear and elongational components present in a comparable amount, approximately. As pointed out above, the plastograph and do-corder have a large elongational zone in the upper part of the mixing cavity. Smoother curves are obtained using the cumulated frequency as a function of the flow type parameter (see Figure 11)

$$\bar{F}(D) = \int_{-1}^{D} \bar{f}(s)\,ds \tag{13}$$

Although the same information is contained in these graphs, this function is bounded since $\bar{F}(-1) = 0$ and $\bar{F}(1) = 1$.

Influence of the operating conditions on the flow type distribution can also be investigated, as will be illustrated in Figure 14, where the cumulated frequencies $\bar{F}$ are shown for different plastograph configurations. The reference configuration is the one used above, whereas the slow speed configuration uses half of the rotation speed of the blades, the half-blade arrangement uses only one side of each blades with

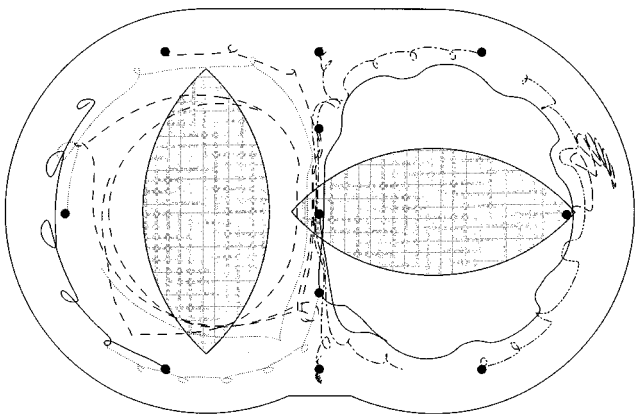

Figure 8. Particle path in the do-corder over three blade rotations.

Initial tracer positions are identified by the filled circles in the mixer.

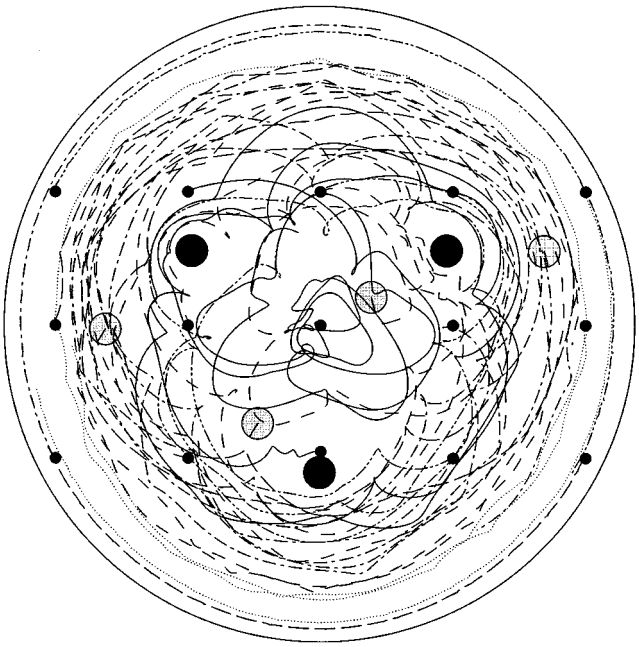

Figure 9. Particle path in the planetary mixer over six rotations of the main supporting arm.

Initial tracer positions are identified by the filled circles in the mixer.

respect to their rotation axis, and finally the large tip clearance has twice the size of the reference one. The results in Figure 14 will suggest that changing the speed or the clearance dimensions does not affect the type of flow inside the mixer. This is not surprising, since one can expect the deformation *intensity* to be affected by changing the speed or the gap dimensions, but not the deformation *pattern*. On the other hand, halving the blades reduces in a sensible way the amount of rotation taking place inside the mixer, which could also be expected, since only half the blades can trap the material into a rotational motion (as will be seen in Figure 13).

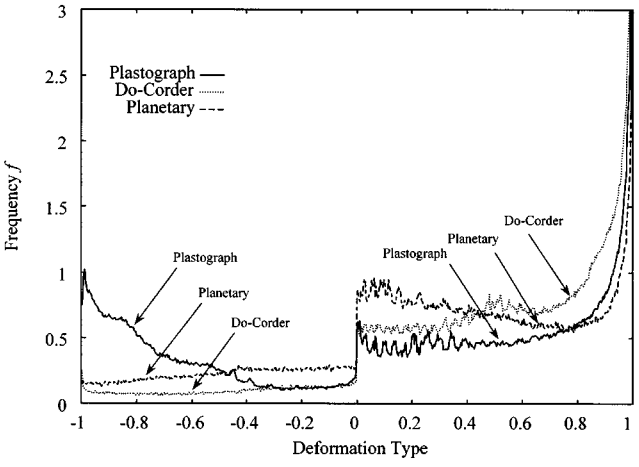

Figure 10. Distribution of the average flow-type parameter in the various mixers.

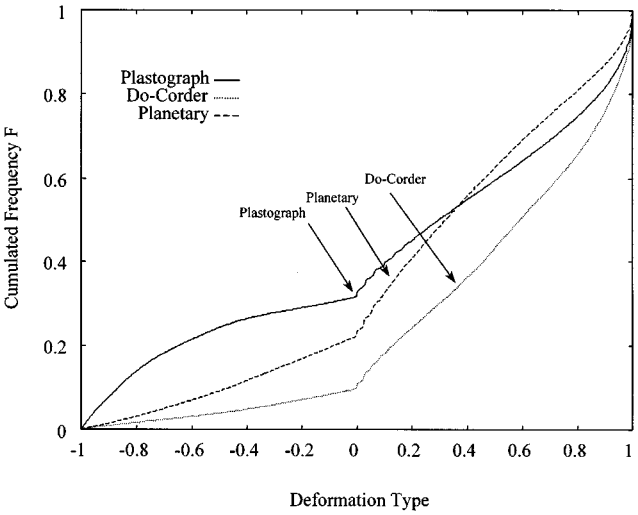

Figure 11. Cumulative distribution of the average flow-type parameter in the various mixers.

Finally, it is possible to characterize the action of the mixers in an even more condensed way, and express it as a single quantity, the time and space average of the parameter D

$$\langle \overline{D} \rangle = \frac{1}{S} \int_{\Omega} \overline{D} dS \tag{14}$$

with

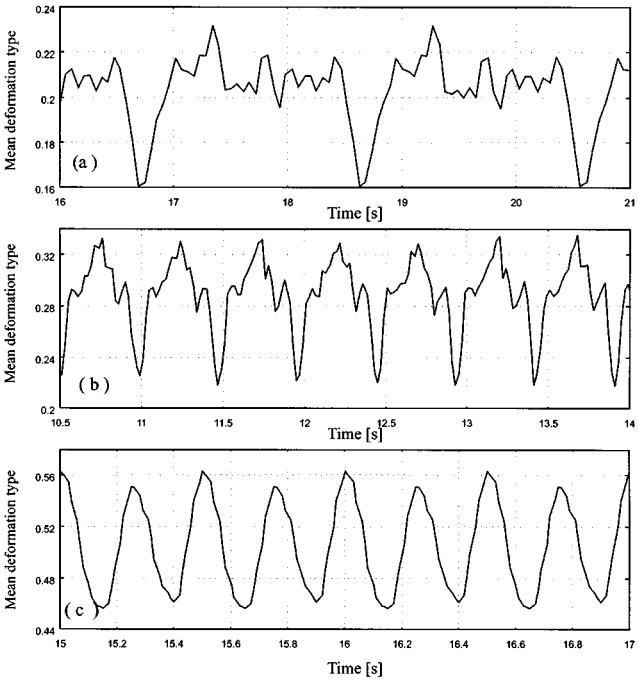

Figure 12. Time evolution of the average flow-type parameter over several mixer rotations.

(a) Plastograph; (b) planetary mixer; (c) do-corder.

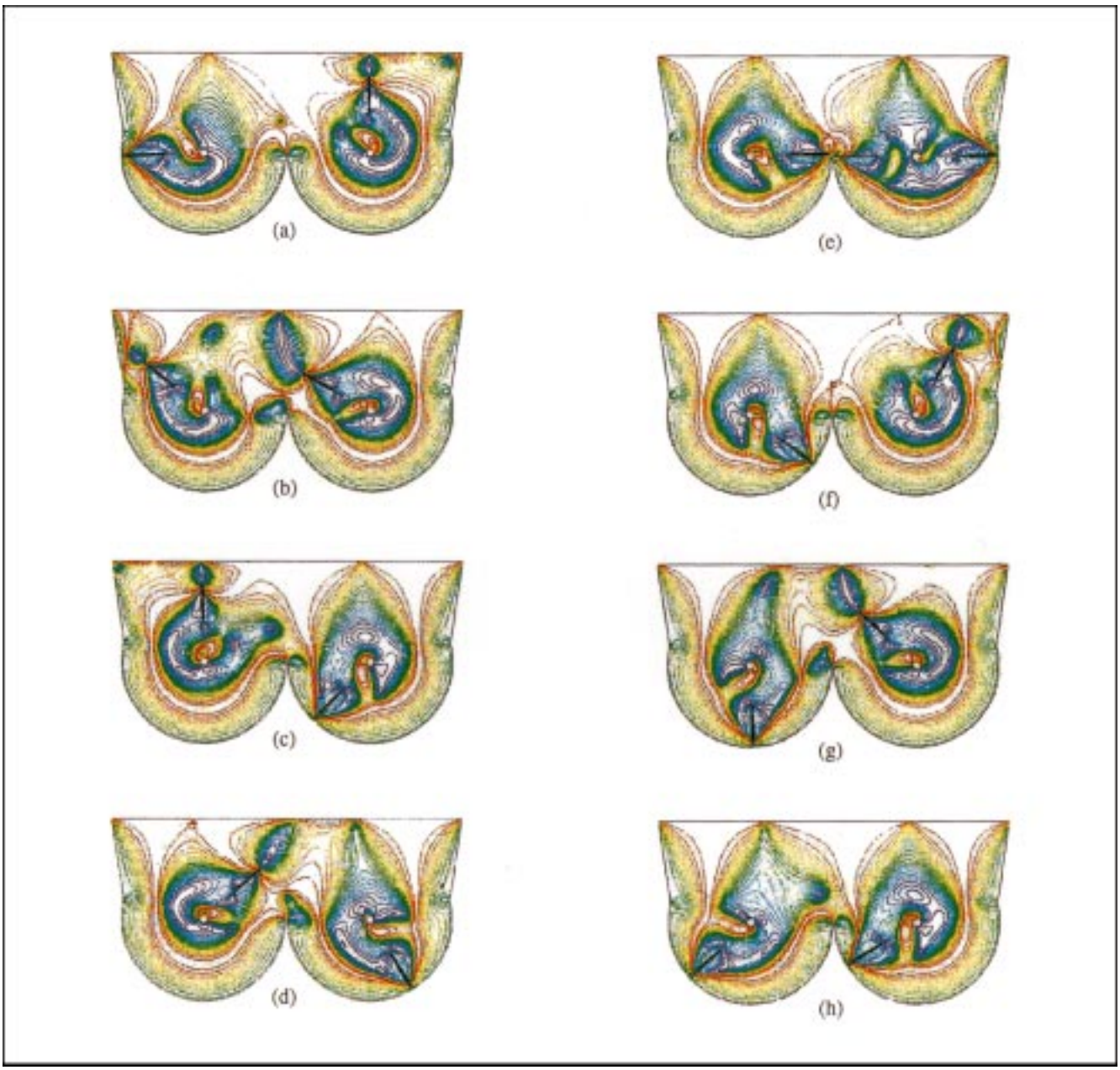

Figure 13. Sequence of instantaneous distributions of the flow-type parameter *D* in the plastograph with half blades over one rotation of the slow blade.

The time interval between the figures is constant, and corresponds to $1/8T$, where T is the period of rotation of the slow blade. Contour values are uniformly distributed within a range between blue (rotation, $D = -1$), green (shear, $D = 0$) and red (elongation, $D = 1$).

$$\overline{D} = \frac{1}{T}\int_0^T D dt \qquad (15)$$

Of course, this single time and space-averaged scalar quantity cannot replace the information contained in the whole complicated spatio-temporal distribution of the flow type parameter D, and comparisons between mixers based solely on this scalar value could be very misleading. For instance, the spatial homogeneity of mixing in a good mixer can be improperly overlooked, or some localized events (in space and/or time) could significantly bias the average and lead to erroneous conclusions. Bearing this in mind, the value of $\langle \overline{D} \rangle$ is given in Table 1 for the mixers considered here. Again, we deduce that the do-corder has the most elongation, and the plastograph and planetary mixers have the most shear contribution.

Conclusions

It has been shown how fluid-flow simulations could be used to investigate and characterize the type of deformations tak-

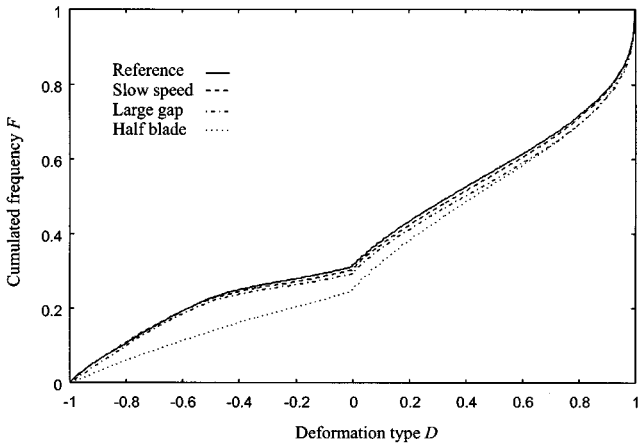

Figure 14. Cumulative distribution of the mean flow-type parameter in the plastograph for various configurations of the mixer blade or rotation speed.

ing place during mixing of high viscosity pastes. For this, relevant flow type criteria have been discussed and computed for different mixer geometries. Based on the different statistics used to analyze and summarize the information about flow characteristics obtained by the simulations, clear differences between the mixers were identified. This analysis can be extended to any type of mixer configuration or any non-Newtonian rheology, and can be used to assess and design mixing equipment in a more objective and rigorous way.

Table 1. Values of the Space and Time Average of the Deformation Parameter D for Different Mixers

Mixer Type	$\langle \overline{D} \rangle$
Plastograph	0.183
Do-corder	0.504
Planetary mixer	0.288

Literature Cited

Astarita, G., "Objective and Generally Applicable Criteria for Flow Classification," *J. Non-Newt. Fluid Mech.*, **6**, 69 (1979).

Bertrand, F., P. A. Tanguy, and F. Thibault, "A Three-Dimensional Fictitious Domain Method for Incompressible Fluid Flow Problems," *Int. J. Numer. Meth. Fl.*, **6**, 719 (1997).

Bird, R. B., R. C. Armstrong, and O. Hassager, *Dynamics of Polymeric Liquids—Fluid Mechanics*, Vol. 1, Wiley, New York (1977).

Buchholz, R. H., "An Epitrochoidal Mixer," *Math. Scientist*, **15**, 7 (1990).

FIDAP Theory Manual, Rev. 7, 1st ed., Fluid Dynamics International (1993).

Glowinski, R., T. W. Pan, and J. Periaux, "A Fictitious Domain Method for Dirichlet Problem and Applications," *Comp. Meth. Appl. Mech. Eng.*, **111**, 283 (1994).

Godfrey, J. C., *Mixing of High-Viscosity Fluids, in Mixing in the Process Industries*, N. Harnby, M. F. Edwards, and A. W. Nienow, eds., Butterworths, London (1986).

Huigol, R. R., "Comments on Objective and Generally Applicable Criteria for Flow Classification by G. Astartia," *J. Non-Newt. Fluid Mech.*, **7**, 91 (1980).

Irving, H. F., and R. L. Saxton, "Mixing of High Viscosity Materials," *Mixing Theory and Practice*, V. W. Uhl and J. B. Gray, eds., Vol. 2, Academic Press, London, p. 169 (1967).

Kawaguchi, Y., M. Kaminoyama, K. Nishi, and M. Kamiwano, "Analysis of Mixing Process For Wet Particle System in a Double Blade Batch Kneader Mixer," *J. Chem. Eng. Jap.*, **30**(3), 550 (1997).

Olbricht, W. L., J. M. Rallison, and L. G. Leal, "Strong Flow Criteria Based on Microstructure Deformation," *J. Non-Newt. Fluid Mech.*, **10**, 291 (1982).

Ottino, J. M., *The Kinematics of Mixing*, Cambridge University Press, Cambridge (1989).

Schunk, P. R., and L. E. Scriven, "Constitutive Equation for Modelling Mixed Extension and Shear in Polymer Solution Processing," *J. Rheol.*, **34**, 1085 (1990).

Tanguy, P. A., R. Lacroix, F. Bertrand, L. Choplin, and E. Brito-De La Fuente, "Finite Element Analysis of Viscous Mixing in a Helical Ribbon Screw Impeller," *AIChE J.*, **38**, 939 (1992).

Tanguy, P. A., F. Bertrand, R. Labrie, and E. Brito-De La Fuente, "Numerical Modelling of the Mixing of Viscoplastic Slurries in a Twin-Blade Planetary Mixer," *TransIChemE*, **74**, 499 (1996).

Manuscript received Jan. 20, 2000, and revision received May 1, 2000.